

A new technique for tensile testing of engineering materials and composites at high strain rates

J. Zhou^a, A. Pellegrino^b, U. Heisserer^c, P.W. Duke^d, P.T. Curtis^a, J. Morton^{a,b}, N. Petrinic^b, V.L. Tagarielli^{a,b,*}

- a. Department of Aeronautics, Imperial College London, London SW72AZ, UK
- b. Department of Engineering Science, University of Oxford, Oxford OX1 3PJ, UK
- c. DSM Materials Science Center Urmonderbaan 22, 6167 RD Geleen, NL
- d. Defence Science and Technology Laboratory, Dstl Porton Down, Salisbury, SP4 0JQ, UK

ABSTRACT

A new test technique and bespoke apparatus to conduct high strain rate measurements of the tensile response of materials are presented. The new test method is applicable to brittle solids and composites as well as high-performance fibres, yarns and tapes used in composite construction. In this study the dynamic response of monolithic poly(methyl methacrylate) (PMMA) and unidirectional composites based on Dyneema[®] tape, Dyneema[®] SK75 yarn and Kevlar[®] 49 yarn are explored. The technique allows early force equilibrium and yields valid tensile stress-strain curves, which include part of the elastic material response. The new method also enables investigation of size effects in tape and yarn materials, allowing testing of specimens of arbitrary length.

Keywords: high strain rate, tensile test, fibre, yarn, tape, composites

*Submitted to Proceedings of the Royal Society A:
Mathematical, Physical and Engineering Science, May 2019*

* Corresponding author. E-mail: v.tagarielli@imperial.ac.uk

1. INTRODUCTION

Many engineering applications employ strong and brittle materials, such as ceramics and metallic alloys, as well as a variety of fibre and tape reinforced composites. In cases where the component is subject to extreme dynamic loading, such as in defence, automotive and aerospace applications, the dynamic properties of these materials need to be evaluated to ensure efficient design.

Several techniques have been developed to conduct tests at strain rates up to 10^3 s^{-1} and above, with the Hopkinson bar setup [1] being the most popular and effective test method. However, measurements in a split Hopkinson pressure bar (SHPB) are valid only after force equilibrium of the specimen is achieved, *i.e.* after the specimen's centre of mass starts moving at uniform speed under the action of equal and opposite forces on the ends of the specimen, which allows unique definitions of current stress, strain and strain rate. For ductile elastic-plastic materials, force equilibrium is typically achieved at the onset of the plastic response, so that the elastic response cannot be measured accurately [2]; in some cases equilibrium may not be achieved at all before catastrophic failure of the specimen [3]. Brittle materials are, therefore, difficult or impossible to test with SHPB techniques in tension.

Several authors ([4]-[23]) have struggled to conduct dynamic measurements on the tensile response of high performance fibres and tapes. For these type of materials it is difficult to achieve force equilibrium during SHPB tests, and specimens are typically limited to only a few millimetres (mm) in length. Stress versus strain curves are reported in the literature for high performance fibres. However, no checks on the validity of the data are presented (e.g. [4]). In addition, several problems exist with gripping of the ends of specimens; these can be solved at low strain rate by employing Capstan Grips (details of the application of such grips in quasi-static tests can be found in [5]). However, such heavy grips cannot be employed in dynamic tests, as their inertia would further delay force equilibrium. Tan *et al.* [6] designed small wedge-action clamps to use in tensile Hopkinson bar experiments, allowing Twaron[®] CT716 fibres to be successfully loaded to failure. Adhesive-based direct gripping methods were adopted to test Dyneema[®] single fibres by Hudspeth *et al.* [7] and Sanborn *et al.* [8]. Hudspeth *et al.* [7] reported uniaxial tensile testing of Dyneema[®] SK76 fibres, recording failure stresses at strain rates up to 600 s^{-1} but no valid stress versus strain histories. Sanborn *et al.* [8] developed a similar set of grips to characterise the tensile behaviour of Dyneema[®] SK76 single filaments at strain rates up to 10^3 s^{-1} .

An alternative test method for Dyneema[®] fibre yarns was developed by Russell *et al.* [9]: the yarn was wrapped around a mobile semi-circular anvil and fixed pins; subsequently a projectile was fired at the semi-circular anvil, inducing dynamic tension in the yarn. No assessment of force

equilibrium was presented, which was unlikely to have been achieved, due to the high mass of the fixtures compared to that of the specimens. Other authors attempted indirect methods to characterise the dynamic response of high-performance fibres. Drodge *et al.* [10] revised a classic transverse fibre impact experiment to test individual silk fibres. A projectile was fired at a clamped silk fibre strand and the subsequent dynamic response was recorded by high-speed photography. With the help of an approximate analytical model, the authors calculated some of the mechanical properties of the silk filament. The need for complex modelling, and the fact that strain rates are varying with time and are quite low, limit the applicability of this method.

All Hopkinson bar techniques in which the specimen is loaded directly in tension incur an additional problem: to maximise the strain rate, the specimen gauge length has to be small. This prevents assessment of the size dependence of the material response and precludes testing of specimens of relatively large size (longer than 10-30 mm).

In addition to the Hopkinson bar setup and similar impact-driven tests, other dynamic loading techniques based on circumferential tension have been developed. Sedlacek and Halden [11] first suggested the hoop tension concept, applied to experiments at low strain rates. A ring-shaped specimen was placed over an inflatable rubber bulb. The bulb pressure was measured by Bourdon-type gauges and the hoop stress in the specimen determined by simple stress analysis. The authors measured the static tensile strength and elongation of acrylic plastics and ceramics. Holman *et al.* [12] designed a similar apparatus to test SAE 4140 steel at low strain rates; here the hoop tension was induced by a rubber O-ring clamped between rigid parallel surfaces. The failure strength of the material was calculated from the pressure at failure, while the elongation was measured by a tungsten wire wrapped around the specimen. Ainscough and Messer [13] further developed this technique and tested ceramic (uranium dioxide) rings at 500-600°C, under quasi-static conditions; the authors measured stress but not strain in their tests.

Several authors have developed dynamic test methods inducing hoop tension under dynamic conditions. Hoggat and Recht [14] used explosives to force a ring specimen to expand at extremely high strain rates. The explosives generated an impulsive radial stress wave of short duration, which impinged on the specimen and forced it to move outwards, expanding under its own inertia. A high-speed camera was used to film the specimens and debris; only small portions of the stress versus strain histories were obtained with this technique. Using a similar setup, Warnes *et al.* [15] achieved strain rates up to $2.3 \times 10^4 \text{ s}^{-1}$ testing the plastic dynamic response of annealed copper. Maliky and Parry [16] studied the dynamic response of three engineering polymers at a strain rate of 10^4 s^{-1} , while Tang *et al.* [17] tested copper samples using a similar technique.

Such expanding ring techniques create extremely high strain rates. However, they share several limitations: (i) experiments are scarcely repeatable and costly; (ii) they are unable to provide stress versus strain histories of the specimens; (iii) the loading is of highly transient nature.

Zhang and Ravi-Chandar [18]-[21] and Morales *et al.* [22] developed an alternative test method based on electromagnetic forces, achieving a strain rate of $1.5 \cdot 10^4 \text{ s}^{-1}$. A solenoid was placed inside a ring specimen; a high current passed through the solenoid's coils, inducing current in the specimen, leading to a repulsive force, which caused the ring to expand rapidly. Liang *et al.* [23] demonstrated a different technique for aluminium ring specimens. These were filled with soft material which was then impacted, causing expansion of the ring. Again, only a small portion of the dynamic response could be recorded in these experiments.

Inspired by previous attempts at expanding ring techniques for dynamic testing, the authors [24] recently developed a new apparatus suitable for testing of brittle materials, tapes and fibres. It has been demonstrated that this new test method provides, under quasi-static conditions, equivalent results to those obtained via conventional quasi-static test methods. In the present study this new technique is applied to tensile testing at high strain rates. The new method eliminates all limitations discussed above: it removes gripping difficulties, promotes early force equilibrium, and allows testing on specimens of arbitrary gauge length. In addition, it permits the use of similar specimens across wide ranges of strain rates, and it is based on a compact apparatus, suitable for testing under a wide range of environmental conditions. In this study the advantages of this new test method are demonstrated; providing, for the first time: (i) valid data on the rate sensitivity of the stiffness of PMMA, (ii) stress versus strain curves for Dyneema® and Kevlar® fibre yarns, and (iii) stress versus strain curves for Dyneema® tapes, at strain rates ranging from quasi-static to 300 s^{-1} .

The structure of the paper is as follows: in Section 2 the materials and specimens tested in this study are described; the apparatus and the high strain rate technique are presented in Section 3; results are discussed in Section 4.

2. MATERIALS AND SPECIMENS

As detailed below, the test method presented here involves securing ring-shaped specimens on a 3D-printed bespoke rubber sleeve. Details of the materials tested and the type of ring specimens manufactured are presented in this Section.

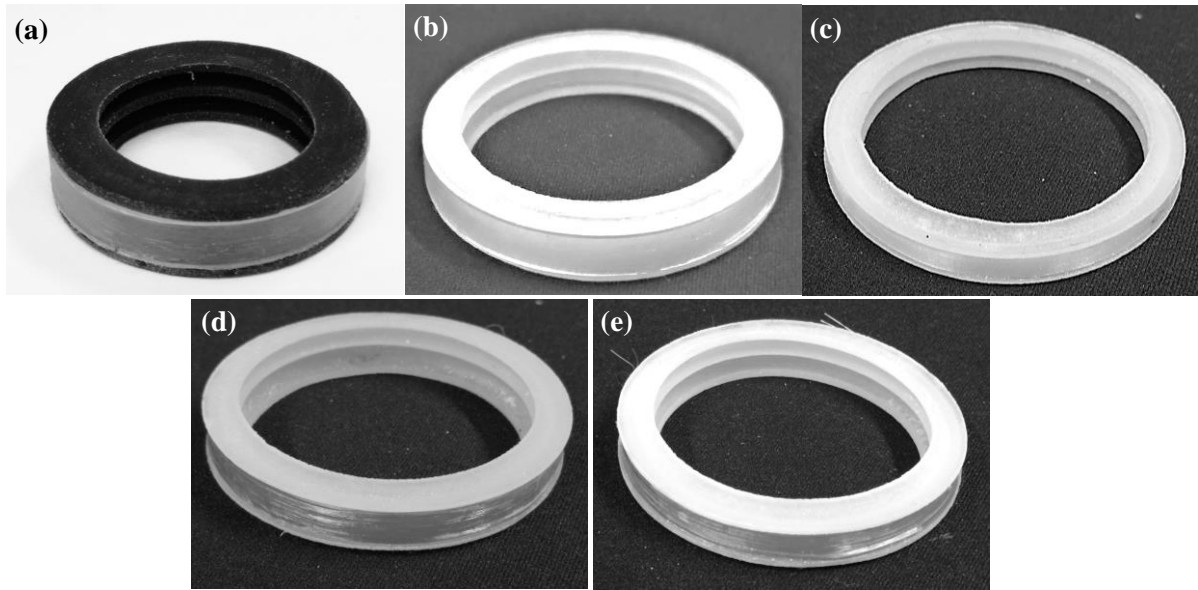


Figure 1. Material specimens tested in this study. (a) PMMA ring, Type I; (b) PMMA ring, Type II; (c) Dyneema[®] tape; (d) Kevlar[®] 49; (e) Dyneema[®] SK75.

2.1 Poly(methyl methacrylate) (PMMA)

Two types of PMMA specimens were tested. Type I ring specimens were machined from an extruded PMMA rod to have 40 mm inner diameter, 1 mm wall thickness and 9 mm height (Figure 1(a)). Two resistance strain gauges were bonded to the outer face of the ring, with an angular spacing of 180°. A second type (Type II) of PMMA rings were machined from an extruded PMMA tube of inner diameter 50 mm with 5 mm wall thickness, to obtain ring specimens having 50 mm inner diameter, 1 mm wall thickness and 6 mm height (Figure 1(b)). Again, the ring specimens were instrumented with two strain gauges. Since the initial rod and tube were obtained from different manufacturers, separate results for the two types of specimens are presented (as they not only have different geometry, but also slightly different mechanical properties).

2.2 Dyneema[®] tape

The high strength DSM Dyneema[®] tape, which is the base material for the cross plied BT10 material, was produced by hot-pressing and calendaring solid state ultra-high molecular weight polyethylene powder (Figure 1(c)). The unidirectional tape is not commercially available and was obtained from DSM; it had thickness of 40 μm and it was cut to a width of 3.5 mm for testing. The tape consisted of unidirectional fibres of ultra-high molecular weight polyethylene, absent any matrix material. (Hot-pressing two layers of tape, with fibres running in perpendicular directions, together with a polyurethane matrix films produces the commercially available cross plied BT10 material.) A

composite ring was constructed by winding several turns of the tape around a rubber sleeve, while spreading cyanoacrylate adhesive on the tape. In all results presented in this paper, the minimum number of two turns of tape was used. This resulted in a composite with a matrix (adhesive) volume fraction of less than 50% in all specimens, such that the effect of the stiffness of the adhesive could be considered negligible. The volume fractions of adhesive and tape were calculated by first weighing the tape and rubber sleeve separately, and then weighing the cured composite assembly. The densities of tape and adhesive were known from the manufacturer's datasheets and confirmed by separate measurements. The effect of the adhesive can be estimated using simple rule-of-mixtures, noting that the adhesive has modulus less than 1 GPa and the stiffness of the tape is two orders of magnitude greater. Therefore, in the data processing we neglect the presence of the adhesive. Two strain gauges of gauge length 10 mm were applied to opposite sides on the surface of the composite ring for hoop strain measurement.

2.3 Kevlar[®] 49 fibre yarn

High strength aramid fibre, Kevlar[®] 49 manufactured by DuPont, was also tested in this study. The fibre yarn consisted of 140 filaments, each of diameter of approximately 12 μm , as estimated from scanning electron microscope (SEM) imaging. The yarn was used to manufacture the composite ring specimen, by winding five turns of the yarn around the rubber sleeve, while applying cyanoacrylate adhesive (Figure 1(d)). The volume fraction of adhesive, measured by weighing the specimens, was less than 50% in all cases. Two strain gauges were bonded to the outer surface of the rubber sleeve, in contact with the inner side of the composite ring specimen.

2.4 Dyneema[®] SK75 fibre yarn

High strength fibre yarn, Dyneema[®] SK75 by DSM, was studied in the present work (Figure 1(e)). The yarn had 100 filaments, each of diameter 17 μm . A composite ring was manufactured and instrumented as detailed above for the Kevlar yarn.

3. TEST APPARATUS AND PROCEDURE

3.1 Details of the apparatus

Two types of test rigs are used in this study, as sketched in Figure 2(a). The assembly on the left is a modification of the prototype presented in [24]. It comprises stainless steel plates bolted together

by four hollow cylinders, to form a frame. This frame supports and constrains two piston/cylinder assemblies, sandwiching a bespoke rubber sleeve, on which the specimen is mounted. The input piston has two holes connecting its ends, allowing the injection of fluid and the evacuation of air bubbles from the fluid generated during setup. The internal part of the rubber sleeve may be filled with a fluid or a soft solid (water was used in this study). The two pistons are then placed in contact with the input and output bars of a compression Hopkinson bar, which is operated in the standard way: following projectile impact, a compressive shockwave propagates down the input bar and piston, pressurizing the fluid and inducing radial expansion of the rubber sleeve and specimen.

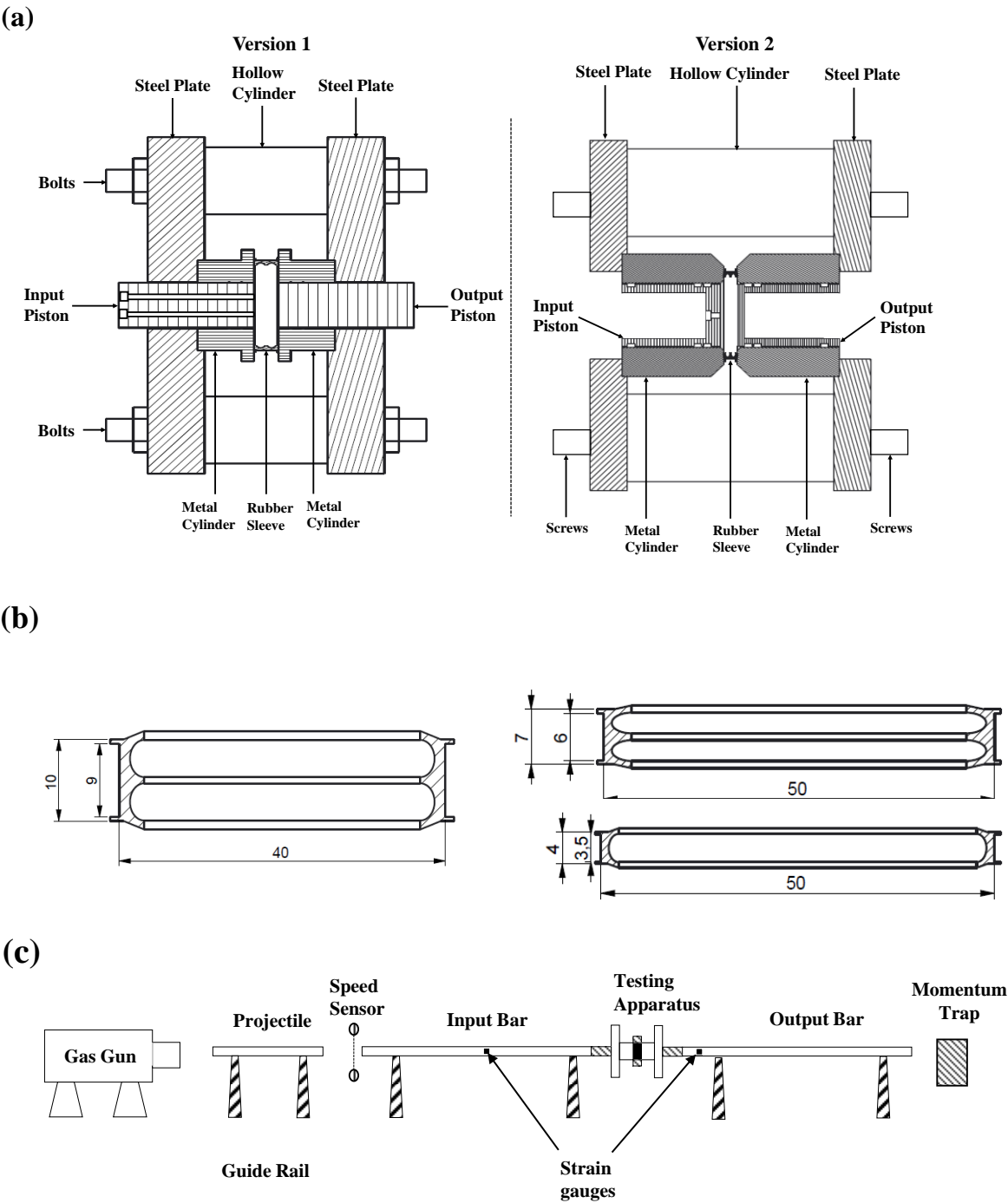


Figure 2. (a) A cross-sectional views of two versions of the apparatus; (b) cross sections of the three types of rubber sleeves used in the tests; (c) Sketch of the SHPB layout used in dynamic testing (not to scale).

The compressive wave is transmitted to the output bar, and measured in both input and output bars, which are instrumented with resistance strain gauges. This set-up allows the two pistons to be positioned a small initial distance (2-10 mm) apart with respect to each other; this reduces the time needed for the forces at the two ends of the apparatus to equilibrate, allowing early measurement of the fluid pressure and, consequently, valid test data in the early stages of the material's response. The same procedure can be used in quasi-static or medium strain rate tests, with loading applied by the cross-heads of an appropriate test machine.

The second type of test rig, on the right-hand side of Figure 2(a), is a version of the apparatus optimised for dynamic testing. Compared to the first version, the diameters of ring specimen, rubber sleeve and pistons were increased, while the height of rubber rings and specimen were reduced, to maximise the circumferential strain rate in the specimen for a given impact velocity. Preliminary tests showed that the stability of the specimen was also improved by high values of the aspect ratio diameter/height. The rig was designed such that an impact at velocity of 20 m/s corresponds to a strain rate in the specimen of 10^3 s^{-1} ; tests at strain rates up to 300 s^{-1} are presented in this study. The pistons were made hollow, to minimise disturbances to the propagation of the loading wave, and were supported by multiple O-rings along their cylinders, to facilitate impact loading. The second rig was constructed in Ti64, for better resistance of the impact forces.

The sequence of events occurring in the test is complex: shock loading of the input piston by the input bar of the SHPB causes a shock in the water, which, propagating axially and radially, interacts with the stiff metallic surfaces and the softer inner surface of the rubber sleeve. Such interaction is of transient nature and may result in fluid cavitation (see e.g. [25]-[27]), which can complicate the interpretation of the test data. Finite element analyses were performed to examine in detail the operation of the apparatus. These, omitted for brevity, showed that within the range of operation of a SHPB (impact velocity not exceeding 20 m/s), the extent of cavitation and the effects of fluid inertia were negligible, and the compressive stress in the bars equals the hydrostatic pressure in the fluid after force equilibrium.

Figure 2(b) shows the three types of rubber sleeves used in this study. The cross-sections contain outer lips, to help position the sample, and inner lips to facilitate sealing. The sleeve on the left corresponds to the first version of the test rig; it has an average wall thickness 3 mm, height

10 mm and outer diameter 40 mm. The two sleeves on the right, with outer diameter 50 mm, average wall thickness 2 mm and height 7 mm or 4 mm, were used with the second version of the apparatus. The sleeve with smaller height was found to be best for testing tapes and yarns; this was due to the fact that, due to the high pressure necessary to bring tape and yarn specimens to failure, during the test the rubber displayed non-uniform radial displacements, invalidating the measurements; this was less evident and problematic for the rubber sleeve with smaller height. The rubber sleeves are manufactured by 3D printing (utilising a Stratasys Connex3) from a polymer blend of ‘TangoBlack’ and ‘VeroWhite’, resulting in a low-porosity elastomer of modulus 10 MPa and Poisson’s ratio 0.48 (at a strain rate of 10^{-3}s^{-1}).

Loading was performed by a SHPB ([28]) sketched in Figure 2(c). This consisted of a gas gun, a Ti64 projectile of length 2.6 m and diameter 16 mm, a Ti64 input bar of length 2.5 m and diameter 16 mm, and a PMMA output bar of length 2 m and diameter 20 mm. The use of a polymeric output bar allowed a more accurate measurement of the dynamic strain. The input bar had multiple strain gauges of gauge length 1 mm at its mid-section, while strain gauges on the output bar were mounted just a few diameters from the impacted end, to minimise wave distortion in the viscoelastic material [29]; a momentum trap was mounted at the opposite end of the output bar. The strain gauges had a gauge length of 1mm to limit the averaging of the strain in the longitudinal direction.

3.2. Test procedure

The test procedure was as follows. First, the ring specimen was placed around the appropriate rubber sleeve; the assembly was inserted between the two metallic cylinders, after lubrication at the rubber-steel interfaces; the two cylinders (sandwiching the assembly of specimen and rubber sleeve) were positioned in the frame. This involved a slight axial compression of the rubber sleeve of order of 2%, which assisted sealing; this also induced a circumferential pre-strain in the specimen, which was monitored by strain gauges and minimized by increasing the cross-section of specimen. The output piston was then inserted in its cylinder; water was introduced to the inner part of the rubber sleeve and part of the input cylinder. The input piston was then inserted in its cylinder and pushed to evacuate any residual air and excess water through the bleed valve(s), which were then closed with M2 screws.

The apparatus was placed horizontally and in contact with the input and output bars. The projectile was fired at velocities up to 8 m/s, and strain gauge signals were recorded by sets of Fylde high-bandwidth amplifiers and Tektronix digital oscilloscopes.

Note that in this paper the response of dry fibre yarns is not measured, since this requires appropriate gripping; instead, unidirectional yarn composites were tested, by adding a cyanoacrylate matrix. For the interested reader, the procedure for gripping dry fibre yarns is outlined in [24].

3.3 Analysis of data

Consider a slender bar of density ρ , Young's modulus E , cross-section A , and speed of sound c_s . Assuming 1-D wave propagation and considering momentum conservation, the strain pulse induced by the impact of the projectile of same cross-section and same material as the input bar with velocity V_0 is:

$$\varepsilon = \frac{V_0}{2c_s} \quad (1)$$

and the corresponding level of stress is:

$$\sigma = E\varepsilon = \frac{\rho c_s V_0}{2} \quad (2)$$

In the test, part of the compressive incident wave $\varepsilon_I(t)$ is reflected back at the interface between input bar and test rig ($\varepsilon_R(t)$), and the rest is transmitted to the output bar, $\varepsilon_T(t)$. The axial displacements at the ends (1 and 2) of the test rig are

$$u_1(t) = c_s \int_0^t \varepsilon_I(\tau) d\tau = c_s \int_0^t (\varepsilon_I - \varepsilon_R) d\tau \quad (3)$$

$$u_2(t) = c_s \int_0^t \varepsilon_2(\tau) d\tau = c_s \int_0^t \varepsilon_T d\tau \quad (4)$$

and the axial “strain” in the test rig can be calculated as:

$$\varepsilon_s = \frac{u_1 - u_2}{L_s} = c_s \int_0^t (\varepsilon_I - \varepsilon_R - \varepsilon_T) d\tau \quad (5)$$

where L_s is the initial distance between the outer ends of the two pistons. The axial loads in the bars (at the ends of the test apparatus) are

$$F_1(t) = (EA)_I [\varepsilon_I(t) + \varepsilon_R(t)] \quad (6)$$

$$F_2(t) = (EA)_O \varepsilon_T(t) \quad (7)$$

At force equilibrium $\varepsilon_I + \varepsilon_R \approx \varepsilon_T$ and Eq.(5) reduces to

$$\varepsilon_s = -\frac{2c_s}{L_s} \int_0^t \varepsilon_R d\tau \quad (8)$$

Figure 3 represents typical force and strain rate histories recorded in a test on a PMMA ring. Forces equilibrate after approximately $100 \mu\text{s}$, corresponding, in this case, to a tensile strain in the specimen of about 0.5%. The strain rate tends to decrease during the test, in this case from approximately 40 s^{-1} at equilibrium to 20 s^{-1} . The variability of strain rate can be corrected by employing appropriate pulse-shaping. However, this was not pursued in this initial study. Knowledge of the forces in the bars allows calculation of the fluid pressure $p_0 = F / A_0$, with A_0 cross-sectional area of the pistons. To estimate the hoop stress in the specimen, consider the free-body diagram in Figure 4, with rubber sleeve and specimen modelled as solids of revolution with rectangular cross-section. The fluid is enclosed by the rigid metal cylinders, pistons and an approximately cylindrical rubber sleeve of inner radius R_0 , outer radius R_i and height h_R ; the specimen has height h_S . The rubber sleeve and specimen expand radially, and their axial strain is restricted by the presence of the rigid metal cylinders.

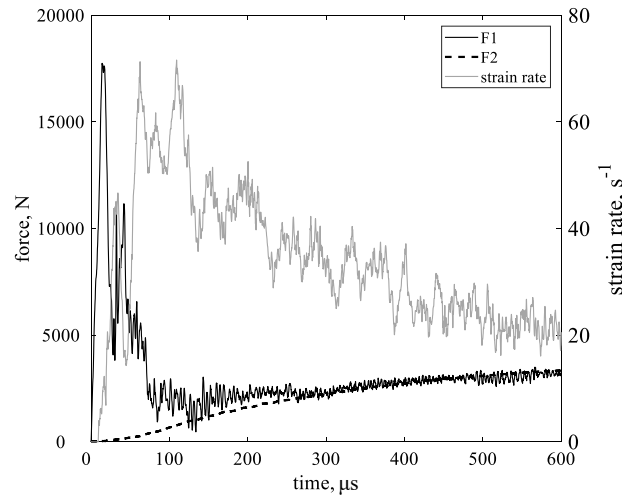


Figure 3. Time history of strain rate and forces on the incident (F1) and output piston (F2), for a test on PMMA (impact velocity of 4.5 m/s). Time $t = 0$ refers to the instant of arrival of the loading wave at the loading piston/water interface.

Pressure at the interface between rubber sleeve and material specimen is p_i , while σ_S and σ_R are the average hoop stresses in the specimen and rubber sleeve, respectively; $\rho_S A_S \ddot{r}$ and $\rho_R A_R \ddot{r}$ denote the inertia forces per unit length, where r is the current radial position of the interface, A_S and A_R are the cross-sectional areas of specimen and rubber. Let $f(p_{axial})$ represent the friction on the rubber sleeve, which is modelled as dependent only on the axial pressure p_{axial} . A first order

analysis of this problem can be performed assuming thin-walled cylinders, negligible friction and inertia after force equilibrium (these effects will be discussed in the Appendix).

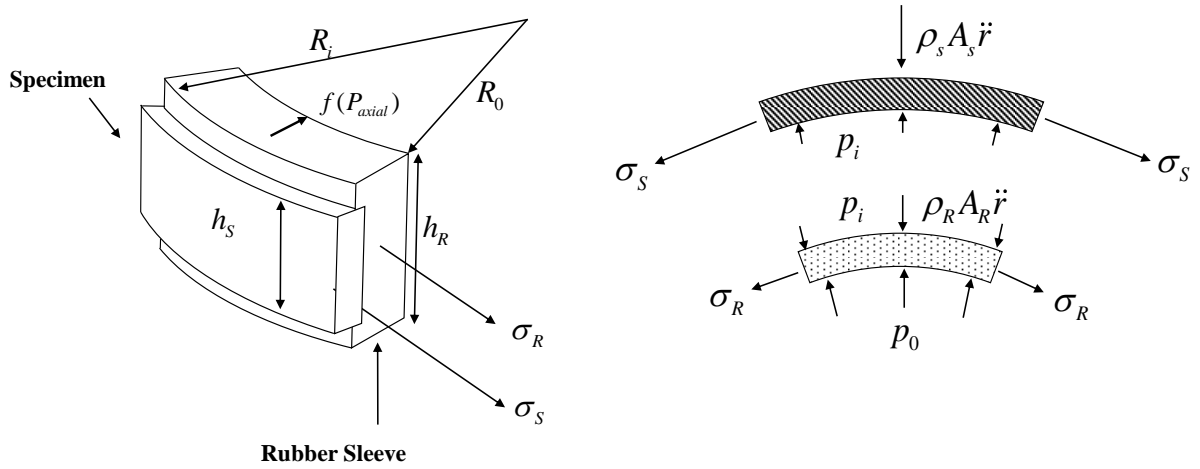


Figure 4. Geometry and free-body diagram of the active part of the apparatus.

Force equilibrium in the specimen dictates

$$\sigma_s A_s = p_i R_i h_s \quad (9)$$

Similarly, the force equilibrium in the rubber sleeve implies that

$$\sigma_R A_R + p_i R_i h_s = p_0 R_0 h_0 \quad (10)$$

The constitutive response of the rubber sleeve in the hoop direction is denoted as $\sigma_R = \sigma_R(\varepsilon)$ and was measured in a set of calibration experiments at different strain rates. Combining Eqns. (9) and (10), the hoop stress in the specimen is obtained as

$$\sigma_s = \frac{1}{A_s} \left[\frac{R_0 h_R F}{A_0} - A_R \sigma_R(\varepsilon) \right] \quad (11)$$

The solid PMMA specimens had rectangular cross-section and $A_s = h_s t_s$, where t_s is the thickness of the specimen; for composite rings the total cross-section depends on the number of windings N , such that $A_s = N A_F$, where A_F is the cross-sectional area of the yarn or tape (and neglecting the presence of cyanoacrylate glue). The value of A_F was measured by embedding the yarn in an acrylic polymer and measuring the number of fibres and their average diameter by analysis of optical micrographs, after appropriate sectioning and polishing.

The apparatus was designed to operate at maximum fluid pressures of order 50 MPa; in this regime the compressibility of the water can be neglected; the rubber used for the sleeve has Poisson's

ratio around 0.48. Therefore, its compressibility can also be neglected in first approximation. Assuming small displacements, the hoop strain ε_h induced in the specimen can be related to the piston displacement δ by

$$\delta A_0 = 2\pi R_i h_R \varepsilon_h R_i \Rightarrow \varepsilon_h = \frac{\delta A_0}{2\pi R_i^2 h_R} \Rightarrow \dot{\varepsilon}_h = \frac{\dot{\delta} A_0}{2\pi R_i^2 h_R} \quad (12)$$

In the preliminary design and tests, the above equation was useful in estimating the strain rate in the specimen from the geometry of the apparatus.

4. RESULTS AND DISCUSSION

The results of the dynamic measurements are summarised in Table 1. Quasi-static tests on these materials were conducted and presented in Zhou *et al.* [24], using the same test rig and slower loading provided by an Instron tensometer operated in compression mode. The static responses are presented with the dynamic data for comparison, and to deduce the strain rate sensitivity of the materials tested. Note that the stiffness in dynamic tests was estimated as the ratio of stress and strain at the point of force equilibrium.

4.1 Calibration tests

A preliminary set of tests were conducted on the rubber sleeve in absence of any specimen. The hoop strain was measured by strain gauges positioned on the outer surface of the rubber sleeve and the stress calculated from Eqn.(11). Figure 5(a) presents the hoop stress vs strain histories at different strain rates. The rubber undergoes a non-linear response, with an initial stiffness and flow stress strongly dependent on strain rate. The data in Figure 5(a) were used to calibrate the response $\sigma_R(\varepsilon)$ in Eqn.(11). It is noted, however, that the second term of the difference in Eqn.(11) was often negligible in the experiments conducted in this study, even at the highest strain rates.

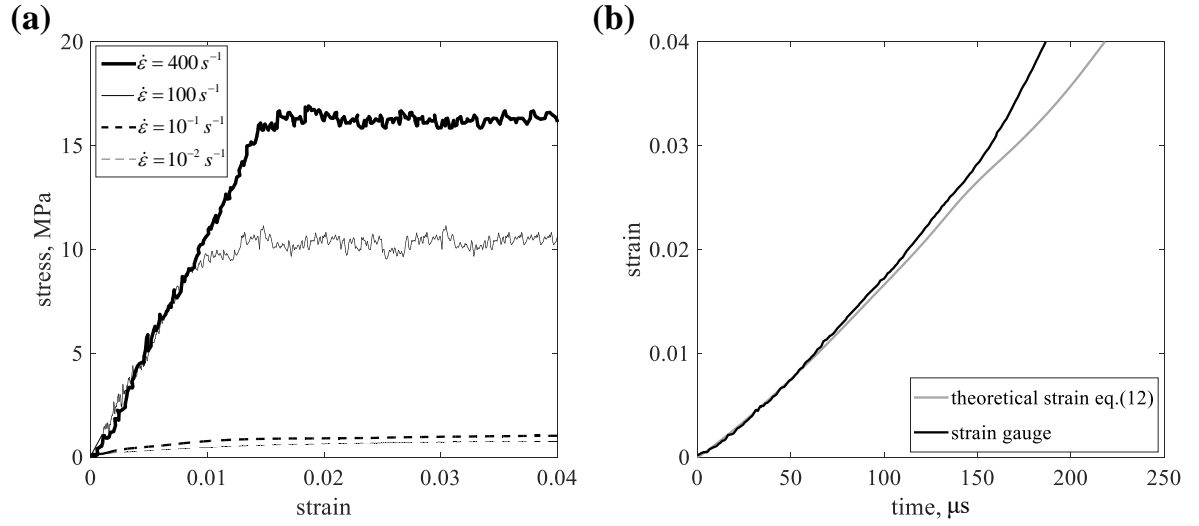


Figure 5(a). Circumferential stress versus strain histories measured at different strain rates for the rubber sleeve in absence of specimens; (b) Measured strain history compared to the predictions of Eqn. (12) at strain rate of 400 s^{-1} .

Table 1. Summary of mechanical properties obtained from the experiments.

material	strain rate (s^{-1})	stiffness (GPa)	strength (MPa)	ductility
PMMA Type I	10^{-3}	3.43	83	0.038
	10^{-2}	3.57	88	0.030
	32	8.8	181	0.020
	46	12.2	223	0.019
	59	14.6	224	0.017
PMMA Type II	10^{-4}	5.03	71	0.018
	10^{-3}	5.3	75	0.016
	111	6.1	97	0.019
	297	6.6	90	0.017
Dyneema [®] Tape	10^{-4}	130	1273	0.011
	10^{-3}	156	1422	0.011
	10^{-2}	156	1689	0.010
	15	175	1775	0.008
	32	201	1846	0.009
	88	214	2176	0.010
	111	230	2260	0.010
Kevlar [®] 49 fibre yarn	10^{-3}	131	2619	0.024
	10^{-2}	160	2817	0.024
	110	167	3151	0.018
	138	177	3379	0.020

Dyneema® SK75 fibre yarn	226	189	3932	0.019
	323	217	3785	0.018
	10^{-4}	112	3054	0.030
	10^{-3}	117	3139	0.029
	72	122	3201	0.026
	76	135	3689	0.030
	129	135	3815	0.031
	204	146	4167	0.029
	209	160	3944	0.028

Figure 5(b) presents the strain history as measured by strain gauges attached to the rubber sleeve, compared to the theoretical predictions of strain from Eqn.(12), and showing that this is accurate up to strains of order 3%. The divergence for $\varepsilon_h \geq 3\%$ is a consequence of non-uniform deformation of the rubber sleeve.

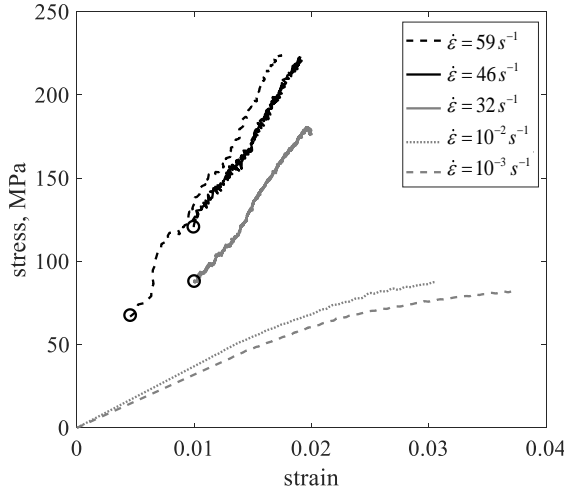


Figure 6. Tensile response of PMMA (Type I) and its sensitivity to strain rate. The circles indicate points of force equilibrium in dynamic tests.

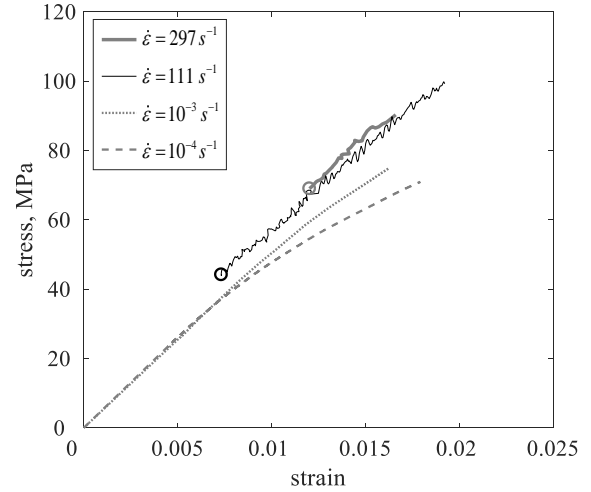


Figure 7. Tensile response of PMMA (Type II) and its sensitivity to strain rate. The circles indicate points of force equilibrium in dynamic tests.

4.2 Response of PMMA

Figure. 6 contains the stress-strain response of PMMA (Type I) for several strain rates, in the range $10^{-3} s^{-1}$ to $60 s^{-1}$. The reference quasi-static data [24] are shown as grey dotted/dashed lines in the plot. The stress-strain curves obtained in the dynamic tests are plotted only beyond the point of force equilibrium, indicated by a circle; hence the entire curves represent valid measurements. Note that the strain rates quoted below are approximate time averages calculated from the point of force equilibrium to the time of failure. The relatively early equilibrium allowed assessment of part of the

dynamic elastic response. The material exhibits strong strain rate sensitivity; it transitions from a non-linear elastic-plastic behaviour at quasi-static loading to a response closer to elastic-brittle at higher strain rates. Figure 7 presents the tensile response of the larger PMMA rings (Type II), showing that the tensile response of this material is significantly less sensitive to strain rate than PMMA Type I. This is possibly due to the fact that Type I specimens were manufactured from an extruded rod of large diameter, while Type II specimens were machined from a thin-walled extruded tube. The measurements of strength and ductility are in line with those reported by other authors (e.g. [30]) for similar polymers.

4.3 Response of Dyneema® Tape

Figure 8 presents the measured tensile response of the Dyneema® tape, indicating a considerable strain rate sensitivity of this material in the range investigated. These stress/strain measurements show that the proposed technique is capable of capturing valid dynamic stress-strain data at very low strain levels and, therefore, suitable for brittle materials like composites and ceramics, as long as they can be manufactured in ring form. It is also noted that the tape tested retains ductility across the strain rate range investigated, which is a desirable property. At all strain rates the material response was approximately linear until failure, which occurred by fibre failure at a cross-section of the specimen-rubber sleeve assembly. To the best of the authors' knowledge, similar tests on this material have not been performed before and are presented for the first time in this paper.

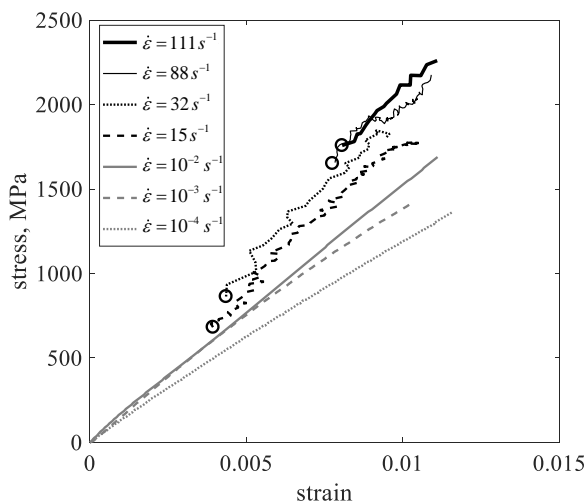


Figure 8. Tensile response of Dyneema® tape composites and its sensitivity to strain rate. The circles indicate points of force equilibrium in dynamic tests.

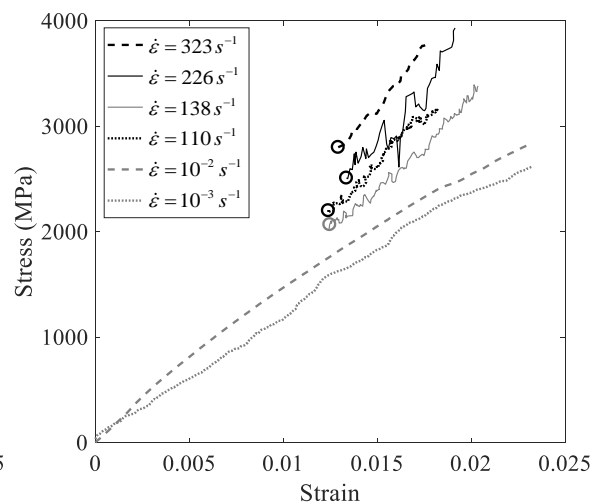


Figure 9. Tensile response of Kevlar® 49 yarn composite and its sensitivity to strain rate. The circles indicate points of force equilibrium in dynamic tests.

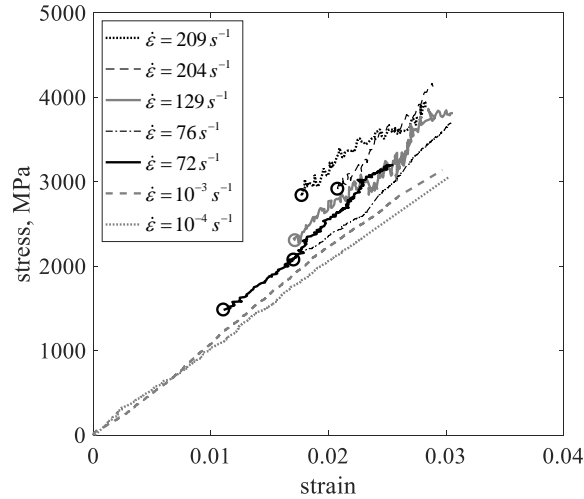


Figure 10. Tensile response of Dyneema® SK75 yarn composite and its sensitivity to strain rate. The circles indicate points of force equilibrium in dynamic tests.

4.4 Response of Kevlar® 49 fibre yarn

Results for composites made from this yarn are shown in Figure 9 and are in line with previous measurements by Wang and Xia [4]. Equilibrium in these tests occurs relatively late. However, the approximately linear material response allows inference of dynamic stiffness (force equilibrium is considered to have been achieved when the 2 forces differ by less than 5%). Kevlar® is less stiff than the Dyneema® tape, but possesses higher strength and ductility. The material exhibits a mild reduction in ductility with increased strain rate. However, the failure mechanisms did not vary with strain rate and always consisted of localised fibre tensile failure.

4.5 Response of Dyneema® SK75 fibre yarn

The results for this material are presented in Figure 10. Measurements show responses with a pronounced sensitivity to the applied strain rate. This material outperforms Kevlar® in ductility, with the difference becoming less evident at higher strain rates. In contrast to Kevlar®, this yarn retains its relatively high ductility across all strain rates investigated. This yarn is notoriously difficult to test, and several authors have attempted measuring its mechanical response. At low strain rate (10^{-3} s^{-1}), the measured strength (3.2 GPa) is in line with that reported by some authors ([7], [8]) but higher than those reported by [9] (2.1 GPa). The measured modulus was in line with [9] (116 GPa) and greater than that found in [8].

At the highest strain rate in this study (200 s^{-1}) a stiffness of 153 GPa and strength of 4.01 GPa were measured, well above the values provided by [9] (modulus 130 GPa, strength 2.7 GPa at strain

rate of 10^3 s^{-1}). The strength values also exceed those in [7] (3.6 GPa at 400 s^{-1}) and [8] (3.5-4.0 GPa at strain rate 600 s^{-1}). The fact that the measured strengths exceed those found in other studies for the same material suggests that the proposed test method reduces the problems encountered by other authors, related to difficulties and stress concentrations induced by gripping as well as to incorrect stress measurements due to absence of force equilibrium. The measurements of the dynamic stiffness of this material are, to the authors' best knowledge, the first valid dataset presented in the literature so far.

Figure 11 summarises all measurements presented in this study. As expected, all the polymeric materials tested in the study display mildly increasing stiffness and strength with increasing strain rate. While PMMA and Kevlar show signs of embrittlement at high strain rates, Dyneema tape and yarn retain their ductility at high rates. A power-law in the form of $y = Ax^m$ is fitted to all datasets in Figure 11, and the material constants A , m are presented in Table 2.

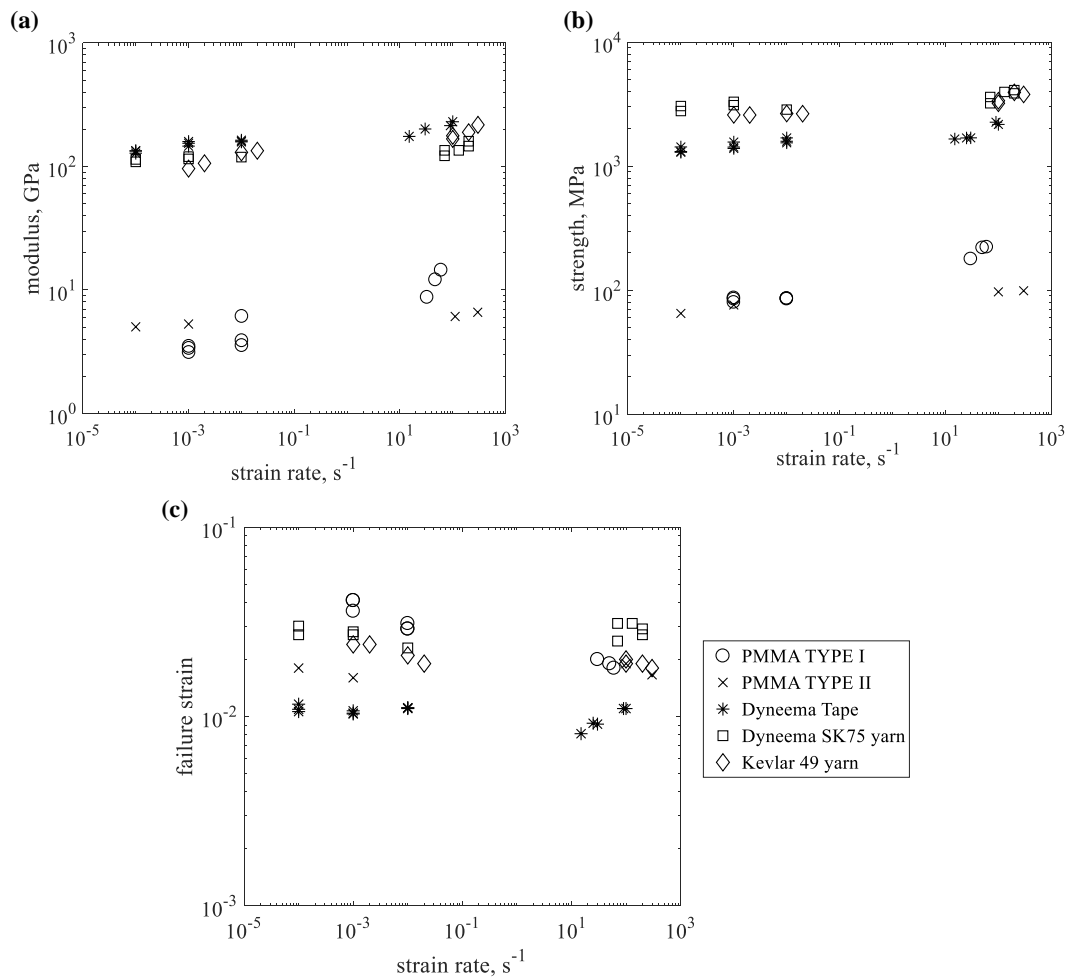


Figure 11. (a). Summary of the sensitivity of material stiffness to applied strain rate; (b) Strain rate sensitivity of the measured material strength; (c) Variation of ductility with the applied

	PMMA (Type I)			PMMA (Type II)			Dyneema Tape			Dyneema SK75			Kevlar 49		
	E	σ	ϵ	E	σ	ϵ	E	σ	ϵ	E	σ	ϵ	E	σ	ϵ
A	7.51	143	0.024	5.86	82	0.017	186	1795	0.010	129	3451	0.028	165	3090	0.020
m	0.117	0.090	-0.064	0.016	0.024	0.002	0.029	0.030	-0.008	0.016	0.018	-0.003	0.026	0.032	-0.016

strain rate. The figure includes power-law fits through the measured data.

Table.2 Material constants A , m obtained from power-law fitting of the datasets in Figure 11. Stiffness (E) is expressed in GPa, strength (σ) in MPa, while ϵ denotes strain at failure.

5. CONCLUSIONS

A new apparatus and associated Hopkinson bar technique for tensile testing of high performance materials across a wide range of strain rates has been presented. The technique allows measurement of valid dynamic stress versus strain histories, solving the long-standing problems of gripping and lack of force equilibrium in the testing of brittle solids and high performance tapes and fibres. The apparatus can be used in combination with different loading devices, ranging from screw-driven tensometers to conventional SHPBs. It allows using a single type of specimen at all strain rates to be investigated. The main conclusions of the study are:

- (i) Force equilibrium is achieved early in the proposed test, allowing estimates of dynamic stiffness at high strain rates; for the first time, these measurements are provided for the four materials tested in this study.
- (ii) Valid dynamic stress versus strain curves are obtained for the first time for the Dyneema[®] tape and SK75 yarn, at strain rates ranging from quasi-static to 323 s⁻¹.
- (iii) The measurements presented here show that, at all strain rates, the dynamic strengths of Kevlar[®] and Dyneema[®] yarns exceed those previously reported in the literature, indicating that the proposed technique is more effective than those appeared so far for the dynamic characterisation of the response of materials.

The proposed apparatus can be easily scaled up or down in size, and different versions can be designed to allow testing of materials with representative volume elements of different size. In the case of tape and fibre materials, the method allows exploration of the size dependence of the response across a range of strain rates, by varying the number of turns of tape, fibres or yarns around the rubber sleeve. The test rig is compact in size (with dimensions not exceeding 200 mm) and can be easily employed in environmentally conditioned atmosphere to explore environmental effects. In principle the test method can be used at strain rates of order 10⁴ s⁻¹, loading by projectile impact

rather than via a SHPB. The investigation of these additional experimental challenges is left to future studies.

ACKNOWLEDGEMENTS

We acknowledge the funding from the Royal Society of London (proof-of-concept project grant, RG130267) and from the Ministry of Defence [dstl] (Technical Partners P. T. Curtis and P. W. Duke). We are grateful to DMS Dyneema® for providing test materials. We are also grateful to M. Jane, S. Carter, J. Meggyesi and S. Del Rosso for assistance with testing and instrumentation.

APPENDIX

The effects of friction and inertia on the operation of the apparatus are analysed in this appendix. Friction acts at the interface between pistons and metal cylinders (via the supporting O-rings), as well as at the interface between rubber sleeve and horizontal surfaces of the cylinders. Both rubber sleeve, specimen and water accelerate substantially during tests at high strain rates, and the associated inertia can potentially affect the test.

Frictional sliding of pistons in their cylinders occurred at a small forces, below 10 N at the fastest speeds investigated. It is noted that this force is negligible compared to the force necessary to break the specimen (in this study force at failure was 3 kN for the weakest specimen - PMMA Type I).

Assuming the rubber sleeve is incompressible ($\nu \approx 0.5$) and applying boundary conditions ($p = -p_0$ at $r = r_0$; $p = -p_i$ at $r = r_i$), Lamé's equations give the distribution of hoop, radial and axial stresses as a function of radial position as

$$\begin{cases} \sigma_h = \frac{p_0 R_0^2 - p_i R_i^2}{R_i^2 - R_0^2} + \frac{(p_0 - p_i) R_0^2 R_i^2}{(R_i^2 - R_0^2) r^2} \\ \sigma_r = \frac{p_0 R_0^2 - p_i R_i^2}{R_i^2 - R_0^2} - \frac{(p_0 - p_i) R_0^2 R_i^2}{(R_i^2 - R_0^2) r^2} \\ \sigma_a = \frac{p_0 R_0^2 - p_i R_i^2}{R_i^2 - R_0^2} \end{cases}, \quad (13)$$

respectively. It is also noted that the axial stress in Eqn. (13) is superimposed to the initial axial compression applied during the assembly of rubber sleeve and cylinders, $P_{init} \approx 0.03$ MPa, considered uniform in first approximation. Friction between the rubber sleeve and the metal surfaces

of the cylinders can be modelled as a radial stress f acting at the top and bottom surfaces of the rubber sleeve, of magnitude proportional to the total axial stress, $f = \mu(P_{init} + \sigma_a)$, where μ is the dynamic friction coefficient between steel and rubber, reported in [31] as 0.25 in case of good lubrication. Note that σ_a varies during the test and in principle it can become tensile, resulting in loss of contact of the rubber sleeve. This can be prevented by employing specimens of stiffness beyond a critical threshold, which was the case in all tests presented here.

Accounting for the frictional force in on the sleeve/specimen system leads to a modified version of Eqn. (11) which reads

$$\sigma_s = \frac{1}{A_s} \left[\frac{R_0 h_R F}{A_0} - A_R \sigma_R(\varepsilon) - \mu(R_i^2 - R_0^2)(P_{initial} + \sigma_a) \right] \quad (14)$$

Making use of Eqn. (13) we obtain

$$\sigma_s = \frac{1}{A_s} \left[\left(\frac{h_R - \mu R_0}{h_s - \mu R_i} \right) \frac{R_0 h_s F}{A_0} - \frac{h_s}{h_s - \mu R_i} A_R \sigma_R(\varepsilon) - \frac{\mu(R_i^2 - R_0^2) h_s}{h_s - \mu R_i} P_{initial} \right]. \quad (15)$$

This new, more accurate equation leads to differences in the calculated stress of at most 5%, compared to Eqn. (11); the stress-strain curves can be corrected to account for this.

When force equilibrium has been achieved $\ddot{r} = \ddot{\varepsilon}_h R_i = 0$ and inertial forces tend to vanish. However, when the strain rate is not constant, Eqn.(11) can be modified to include the inertia of specimens and rubber sleeve, giving

$$\sigma_s = \frac{1}{A_s} \left[\frac{R_0 h_R F}{A_0} - A_R \sigma_R(\varepsilon) - (\rho_R A_R R_0^2 + \rho_S A_S R_i^2) \ddot{\varepsilon}_h \right] \quad (16)$$

The inertial terms in Eqn. (16) were evaluated to less than 0.5% of the first two terms in the equation. The inertia of water was not considered here, as both its mass and its acceleration during the test are relatively low. In conclusion, inertial effects are negligible in the range of operation of a standard SHPB (loading up to 20 ms⁻¹). To simultaneously account for the frictional and inertial effects, stress can be calculated as

$$\sigma_s = \frac{1}{A_s} \left\{ \left(\frac{h_R - \mu R_0}{h_s - \mu R_i} \right) \frac{R_0 h_s F}{A_0} - \frac{h_s}{h_s - \mu R_i} A_R \sigma_R(\varepsilon) - \frac{\mu(R_i^2 - R_0^2) h_s}{h_s - \mu R_i} P_{initial} - \frac{h_s}{h_s - \mu R_i} (\rho_R A_R R_0^2 + \rho_S A_S R_i^2) \ddot{\varepsilon}_h \right\}, \quad (17)$$

which may serve to explore the applicability of the proposed test method to specimens of different size and geometry.

REFERENCES

- [1] Tagarielli VL, Deshpande VS, Fleck NA. The high strain rate response of PVC foams and end-grain balsa wood. *Composites Part B: Engineering* 2008;39(1):83-91. (<https://doi.org/10.1016/j.compositesb.2007.02.005>)
- [2] Pellegrino A, Tagarielli VL, Gerlach R, Petrinic N. The mechanical response of a syntactic polyurethane foam at low and high rates of strain. *Int J Impact Eng* 2015 1;75:214-221. (<https://doi.org/10.1016/j.ijimpeng.2014.08.005>)
- [3] Naik NK, Perla Y. Mechanical behaviour of acrylic under high strain rate tensile loading. *Polym Test* 2008 06;27(4):504-12. (<https://doi.org/10.1016/j.polymertesting.2008.02.005>)
- [4] Wang Y, Xia Y. The effects of strain rate on the mechanical behaviour of kevlar fibre bundles: an experimental and theoretical study. *Composites Part A: Applied Science and Manufacturing* 1998 11;29(11):1411-1415. ([https://doi.org/10.1016/S1359-835X\(98\)00038-4](https://doi.org/10.1016/S1359-835X(98)00038-4))
- [5] ASTM F1106-87 Standard specification for warping heads, Rope Handling (Gypsy Head, Capstan Head). ASTM International, West Conshohocken. 2012; (<https://doi.org/10.1520/F1106-87R12>)
- [6] Tan VBC, Zeng XS, Shim VPW. Characterization and constitutive modeling of aramid fibers at high strain rates. *Int J Impact Eng* 2008 11;35(11):1303-1313. (<https://doi.org/10.1016/j.ijimpeng.2007.07.010>)
- [7] Hudspeth M, Nie X, Chen W. Dynamic failure of Dyneema SK76 single fibers under biaxial shear/tension. *Polymer (United Kingdom)* 2012;53(24):5568-5574. (<https://doi.org/10.1016/j.polymer.2012.09.020>)
- [8] Sanborn B, DiLeonardi AM, Weerasooriya T. Tensile properties of Dyneema SK76 single fibers at multiple loading rates using a direct gripping method. *Journal of Dynamic Behavior of Materials* 2015;1(1):4-14. (<https://doi.org/10.1007/s40870-014-0001-3>)
- [9] Russell BP, Karthikeyan K, Deshpande VS, Fleck NA. The high strain rate response of ultra high molecular-weight polyethylene: from fibre to laminate. *Int J Impact Eng* 2013 10;60:1-9. (<https://doi.org/10.1016/j.ijimpeng.2013.03.010>)
- [10] Drodge DR, Mortimer B, Holland C, Siviour CR. Ballistic impact to access the high-rate behaviour of individual silk fibres. *J Mech Phys Solids* 2012 10;60(10):1710-1721. (<https://doi.org/10.1016/j.jmps.2012.06.007>)
- [11] Sedlacek R, Halden FA. Method for tensile testing of brittle materials. *Rev Sci Instrum* 1962 03;33(3):298-300. (<https://doi.org/10.1063/1.1717827>)
- [12] Holman WR, Stiles EB, Fung E. Tensile test apparatus for small ring specimens. *J Sci Instrum* 1967 07;44(7):545-547.
- [13] Ainscough JB, Messer PF. An apparatus for the tensile testing of ceramic ring specimens at elevated temperatures. *Journal of Physics E (Scientific Instruments)* 1974 11;7(11):937-9.
- [14] Hoggatt CR, Recht RF. Dynamic stress-strain relationships determined from expanding ring experiments. *Experimental Mechanics* 1969, 9 (10): 441-448
- [15] Warnes RH, Karpp RR, Follansbee PS. The freely expanding ring test-a test to determine material strength at high strain rates. *Transactions of the ASME Journal of Engineering Materials and Technology* 1986 10;108(4):335-9. (<https://doi.org/10.1051/jphyscol:1985575>)
- [16] Al-Maliky N, Parry DJ. Measurements of high strain rate properties of polymers using an expanding ring method. *Journal De Physique IV : JP* 1994;4(8):C8-71-C8-76. (<https://doi.org/10.1051/jp4:1994810>)
- [17] Tang T, Ren G, Guo Z, Li Q. An improved technique of expanding metal ring experiment under high explosive loading. *Rev Sci Instrum* 2013 04;84(4):043908 (6 pp.). (<https://doi.org/10.1063/1.4802255>)
- [18] Zhang H, Ravi-Chandar K. On the dynamics of necking and fragmentation - I. Real-time and post-mortem observations in Al 6061-O. *Int J Fract* 2006;142(3-4):183-217.

(<https://doi.org/10.1007/s10704-006-9024-7>)

- [19] Zhang H, Ravi-Chandar K. On the dynamics of necking and fragmentation - II. Effect of material properties, geometrical constraints and absolute size. *Int J Fract* 2008 03;150(1-2):3-36. (<https://doi.org/10.1007/s10704-008-9233-3>)
- [20] Zhang H, Liechti K, Ravi-Chandar K. On the dynamics of localization and fragmentation. III. Effect of cladding with a polymer. *Int J Fract* 2009 02;155(2):101-18. (<https://doi.org/10.1007/s10704-009-9332-9>)
- [21] Zhang H, Ravi-Chandar K. On the dynamics of localization and fragmentation-IV. Expansion of Al 6061-O tubes. *Int J Fract* 2010;163(1-2):41-65. (<https://doi.org/10.1007/s10704-009-9441-5>)
- [22] Morales SA, Albrecht AB, Zhang H, Liechti KM, Ravi-Chandar K. On the dynamics of localization and fragmentation: V. Response of polymer coated Al 6061-O tubes. *Int J Fract* 2011 12;172(2):161-85. (<https://doi.org/10.1007/s10704-011-9654-2>)
- [23] Liang MZ, Li XY, Qin JG, Lu FY. Improved expanding ring technique for determining dynamic material properties. *Rev Sci Instrum* 2013 06;84(6):065114 (5 pp.). (<https://doi.org/10.1063/1.4811658>)
- [24] Zhou J, Tagarielli V, Heisserer U, Curtis P. An Apparatus for Tensile Testing of Engineering Materials. *Exp Mech* 2018;1-10. (<https://doi.org/10.1007/s11340-018-0393-4>)
- [25] Schiffer A, Tagarielli VL. The response of rigid plates to blast in deep water: fluid–structure interaction experiments. *Proceedings of the Royal Society A: Mathematical, Physical and Engineering Sciences* 2012;468(2145):2807-2828. (<https://doi.org/10.1098/rspa.2012.0076>)
- [26] Schiffer A, Tagarielli VL, Petrinic N, Cocks AC. The response of rigid plates to deep water blast: analytical models and finite element predictions. *Journal of Applied Mechanics*. 2012 Nov 1;79(6):061014. doi: (<https://doi.org/10.1115/1.4006458>)
- [27] Schiffer A, Tagarielli VL. The one-dimensional response of a water-filled double hull to underwater blast: experiments and simulations. *International journal of impact engineering*. 2014 Jan 1;63:177-87. (<https://doi.org/10.1016/j.ijimpeng.2013.08.011>)
- [28] Siegkas P, Tagarielli V, Petrinic N, Lefebvre L. The compressive response of a titanium foam at low and high strain rates. *J Mater Sci* 2011;46(8):2741-2747. (<https://doi.org/10.1007/s10853-010-5147-3>)
- [29] Bacon C. Separation of waves propagating in an elastic or viscoelastic Hopkinson pressure bar with three-dimensional effects. *Int J Impact Eng* 1999 01;22(1):55-69. ([https://doi.org/10.1016/S0734-743X\(98\)00048-7](https://doi.org/10.1016/S0734-743X(98)00048-7))
- [30] Wu H, Ma G, Xia Y. Experimental study of tensile properties of PMMA at intermediate strain rate. *Mater Lett* 2004 11;58(29):3681-5. (<https://doi.org/10.1016/j.matlet.2004.07.022>)
- [31] Roth FL, Driscoll RL, Holt WL. Frictional properties of rubber. United States Bureau of Standards -- *Journal of Research* 1942;28(4):439-462.